

Application of machine vision in drying process modeling of carrot slices

Gourab Basu¹, Kshanaprava Dhalsamant¹, Punyadarshini Punam Tripathy^{1,*}, Sonu Sharma²

¹ Agricultural and Food Engineering Department, Indian Institute of Technology Kharagpur, West Bengal 721302, India

² University of Guelph, Ontario, N1G 2W1, Canada

* Corresponding author: Punyadarshini Punam Tripathy, punam@agfe.iitkgp.ac.in

ARTICLE INFO

Received: 4 October 2023

Accepted: 22 December 2023

Available online: 30 December 2023

doi: 10.59400/cai.v1i1.383

Copyright © 2023 Author(s).

Computing and Artificial Intelligence is published by Academic Publishing Pte. Ltd. This article is licensed under the Creative Commons Attribution License (CC BY 4.0).
<http://creativecommons.org/licenses/by/4.0/>

ABSTRACT: In this current research, the drying characteristics of carrot slices dried in a convective hot-air dryer are analyzed employing image analysis to determine the most significant factor. From the acquired images, nine parameters viz. redness (R), greenness (G), blueness (B), lightness (L), redness (a), yellowness (b), energy, entropy, and upper surface area of carrot slices were calculated using the algorithm developed in MATLAB 2015a. Boruta feature selection algorithm in the R console showed lightness, redness, and energy were the most significant features among calculated parameters. Additionally, single-layer feed-forward artificial neural network (ANN) architecture with three inputs (hot air temperature, thickness of slices, drying time), and outputs namely lightness, redness, and energy with one hidden layer was used to model input variables to that of responses. Multiple regression models are employed to optimize the drying condition by further assessing the behavior of response variables with hot air temperature and thickness of slices as inputs and lightness, redness, and energy as outputs. The lightness and redness of samples are found to be decreasing with an increase in temperature and a decrease in thickness. Whereas, the effect of these input parameters on energy, the measure of homogeneity of the product surface, is found to be reversed to that of the effect on lightness and redness. Lightness and redness are set to be highest, whereas energy was kept to be lowest. Convective hot air temperature of 60 °C and 7 mm thickness sample was found to provide the best quality product within the experiment range.

KEYWORDS: machine vision; Boruta; optimization; image analysis; carrot slices

1. Introduction

Carrot (*Daucus carota* L.) is the foremost vegetable plant across the globe owing to its large production of greater than 41 million tons (carrot + turnips)^[1]. Carrot is used as processed or fresh produce for human consumption and contains around 16 to 38 mg/100 g carotenoids. These carotenoids are found to improve our immune system and decrease the risk of a few types of cancer and cardiovascular disease^[2]. It needs to be dried to increase its shelf life, be easy to transport, and assure protected storage due to its perishability^[3-5]. Different techniques like osmotic dehydration, tray drying, fluidized bed, etc. were used to reduce the moisture content of carrots up to safe storage moisture level (9%–10% dry basis)^[6]. The primary interest in these studies has been an investigation of drying kinetics at different operating

conditions and a suitable model describing the process accurately. Optimization of independent operating variables based on chemical (carotene content) and physical parameters (like bulk density and rehydration ratio) was also investigated^[7]. During drying, changes in visual characteristics are prominent^[4]. These include a change in color, texture, and morphology of the product. Thus, to assess the effect of drying on the product, quantification of these qualitative attributes becomes very important^[8]. The color attributes include redness, lightness, yellowness, etc., whereas the texture of visual properties includes energy, homogeneity, contrast, etc., and the morphological properties include area, perimeter, ferret diameter, etc.

Machine vision is a novel, rapid, non-contact, and non-destructive method of quantitative information procurement technique for the object of interest^[5]. The food industry is among the most important sectors where machine vision is employed in a wide range of applications^[9]. Machine vision primarily includes an image acquisition system and a computer system for the analysis of acquired data^[10]. Depending upon the particular interest images may be acquired by hyperspectral camera or charged couple device (CCD) camera or scanning electron microscope^[11], etc. Among all these devices CCD camera-based images are the most widely used^[5]. Images are mostly used to classify the different objects in a mixture. These include different varieties of grains, different grades of fruits^[9,11], etc. Images are also used to monitor the effect of various unit operations on the products being operated^[12]. Batch drying of shrimps, figs, and apples is a few examples of this paradigm of application^[13,14]. Another aspect of the application of machine vision in food is a non-destructive chemical analysis using hyperspectral images^[15].

Machine vision is a technique for quantification of the aforementioned visual properties. Thus, to meet the requirement for quantification of qualitative visual properties, machine vision can play an inevitable role. There has been increased interest in the past decade in the application of machine vision in the food sector application^[5,15-17]. For example, different varieties of wheat grains were classified based on image color, texture, and morphology^[18], an algorithm for the classification of different types of fruits^[19] using a feed-forward neural network (FNN)^[14]. There is another aspect of the application of machine vision that assesses the change of quality attributes like color during an operation. Mass transfer kinetics of osmotically dehydrated kiwi fruits were investigated by Fathi et al.^[20], using image analysis. A study on the effect of drying variables on morphological parameters during convective drying showed a statistically significant relationship between drying medium temperature, velocity, and image texture parameters like normalized energy, contrast, and homogeneity^[21,22].

Color kinetics during hot air drying of the osmotically dehydrated pumpkin using image analysis suggested that image textural and morphological features should be taken into consideration to describe the effect of drying time on the product more precisely^[23]. In another study, the drying condition of apple slices was optimized on the basis of color change, shrinkage, and drying time by image analysis to find out color change and shrinkage^[24].

Image processing and analysis is an innovative tool to recognize objects of interest and for extracting computable data from digital images to deliver objective, non-contact quality assessment without destruction^[25,26].

In food industries, machine vision is used largely for the classification of fruits, meats, cereals, nutrient determination, and moisture content distribution in food products. There has been an increased interest in the application of machine vision in the food processing sector in the past few decades. Some of the important features like the area and total color change of food products have been widely used for

drying process modeling as response variables^[24,27-29]. However, the textural and morphological features should also be taken into account to get a holistic view of the effect of drying on product quality as proposed by Zenoozian et al.^[23]. Different varieties of wheat grains were classified in terms of image color, texture, and morphology^[18]. For image analysis, texture represents the distribution pattern of intensity values of reflected light from the surface, whereas morphology suggests the shape and size of an object of interest. Fernandez et al.^[30] carried out the image analysis of apple discs to assess the impact of laboratory air drying on the color, shrinkage, and texture of the image. They observed that area was reduced during drying whereas the perimeter did not change much. Similarly, redness increased during drying and lightness almost remained the same. Boruta feature selection algorithm is used to choose statistically significant responses from computationally intensive parameters in the simplest form. Poona and Ismail^[31], reported that the Boruta algorithm implanted with a random forest classification algorithm provided a precise model for judicious selection of healthy and infected seedlings. Lim et al.^[32], used the Boruta wrapper algorithm to select essential features for the analysis in order to verify the authenticity of white rice. According to the Boruta algorithm, 13 lysoglycerophospholipids (GPLs) were essential among 17 lysoGPLs, hence 13 lysoGPLs were considered essential for their study.

Recent technological advances have transformed several sectors, including food processing. Carrot slice drying modelling using machine vision is a breakthrough. This revolutionary drying technology offers unmatched accuracy and efficiency. Machine vision uses advanced algorithms and image processing to monitor and analyze drying dynamics in real time, revealing moisture content, shrinkage, and color changes. Machine vision enables predictive modelling during carrot slice drying, improving process control and product quality. This research discusses how machine vision can optimize drying settings and produce high-quality dehydrated carrot products in carrot slice drying. This paper's technique, findings, and comments illuminate machine vision's many uses and implications in carrot slice drying. In doing so, we aim to contribute to the growing body of knowledge at the intersection of food science, technology, and process optimization.

Though drying operation increases shelf life, it also reduces the quality attributes of products. Quality evaluation is often both a destructive and expensive task. In this regard, machine vision can intervene and offer a reasonably good solution.

The incorporation of machine vision into the modelling of carrot slice drying process is a state-of-the-art development in the ever-changing field of food processing^[33]. Utilizing advanced algorithms and real-time picture analysis, machine vision provides an unparalleled degree of accuracy in monitoring and comprehending the drying dynamics^[34]. This study explores the significant advancements introduced by machine vision and conducts a thorough comparison with the most advanced techniques currently available. Through comparing the advantages and disadvantages, our aim is to determine the superiority of machine vision in terms of its ability to forecast outcomes, regulate processes, and improve the overall efficiency of drying carrot slices.

2. Materials and methods

2.1. Raw material

Fresh carrots (*Daucus Carota* L.) were brought from the local market of IIT Kharagpur and kept at 4 °C in the refrigerator. During the experiment, carrots were cut using a vegetable cutter and made into slices of 30 mm diameter (3 mm, 5 mm, and 7 mm thicknesses) and dipped into the water. Finally, carrot slices were kept in a convective tray dryer for drying at preset conditions (50 °C, 60 °C, 70 °C). The initial

moisture content of carrot samples was found to be 85% to 89% (wet basis).

2.2. Convective hot air drying

A laboratory-scale convective hot tray dryer was used for drying carrot slices. Prior to drying, the dryer was run for 30 min to bring the drying air condition to the desired condition under a steady state. Carrot slices were put into the top and middle tray. Experiments were carried in different levels of drying air temperature (60 °C, 70 °C, and 80 °C) and different slice thicknesses (3 mm, 5 mm, and 7 mm) in a laboratory-scale tray dryer with an air velocity of 1.3 m/s. During each experimental run, firstly, a tray having 25 slices of carrots was weighed and put into the dryer. After 15 min the next tray having the same number of carrots was further inserted into the dryer. Thus, after four trays were inserted into the dryer consecutively, the first tray was already treated for 45 min. Now within 15 min of time span, the tray was taken out the dryer, carrot slices were weighed by a weighing balance, and the image was taken by the aid of the image acquisition system. Thus, in 15 min, each tray was taken out of the dryer and the aforementioned measurements were taken. While image acquisition, it was made sure that each time a particular slice is placed on the same position over and over. Thus, the image of particular slices was taken repeatedly. This process ensures proper representation of the image attributes. Otherwise, these attributes will vary. The endpoint of drying was determined when there was no significant variation in the mass of samples in three successive readings.

2.3. Image acquisition and image processing

This section elaborates the steps involved in the image acquisition system and the different steps involved in image processing in detail.

2.3.1. Image acquisition

The image acquisition system was constructed using thermocol and chart paper. Thermocol sheets having a thickness of 2 cm were brought from the market. Two squares of 41 m × 41 m were cut for the base and ceiling of the box. Another four pieces of thermocol were cut in the size of 41 m × 31 m for the sides of the acquisition box. Thus, the overall dimension of the image acquisition box was 41 m × 41 m × 31 m. Green chart paper was used as the background of the image. It was done since the green background has negligible redness whereas the carrot has high redness compared to that of the background. Thus, the red color channel was used to segment the image from the background. A backlit system of illumination was employed. In this regard, strip LED lights were used for illumination purposes. Motorola E (2nd generation) phone was used to capture the image. The phone was placed at the top of the box. There was a hole on the top of the box through which the image was captured. The camera lens had an exposure time of 1/139 seconds and a focal length of 2 mm with an aperture of $f/2.2$. Both horizontal and vertical resolution of the image was 72 dpi with a pixel size of 1920 × 2560. The image was stored in .jpg format.

2.3.2. Image processing

Image processing is done to improve the quality and interpretability of the acquired image. Noise is removed from the image. Thus, actual and appropriate quantification of image attributes is measured. Image processing involves several steps. The applicability of an algorithm that is steps involved in processing depends upon the case-specific requirement. For example, an algorithm used for the classification of different kinds of fruits will be different from an algorithm involved in the modeling of the dehydration process of shrimps. Thus, before incorporating a particular algorithm, it becomes very essential to understand the problem domain properly. This makes the certainty of steps to be taken

properly to yield the desired outcomes.

The different steps involved in the image processing of carrot slices are shown in a flowchart in **Figure 1**. Steps include image acquisition, image filtering, separation of the red channel, segmentation of the separated image, masking of the segmented binary image on the original color image, and finally conversion of masked color image into the gray image. After the involvement of these steps, the original image can be subjected to be quantified. The required image attributes are derived based on the final processed image. Different stages of the image of fresh carrot slices (5 mm thickness) taken for the experiment resulting from each of the mentioned steps are shown in **Figure 2**.

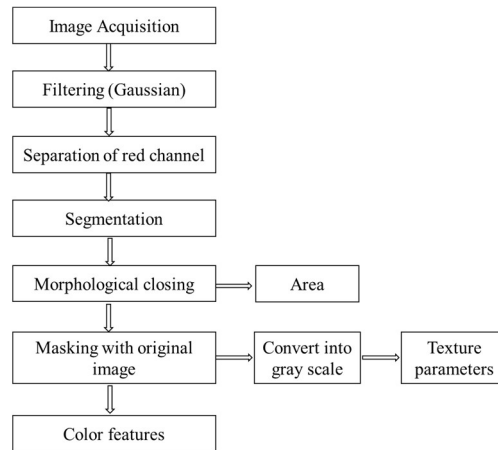


Figure 1. Flowchart of steps involved in image analysis of carrot slices.

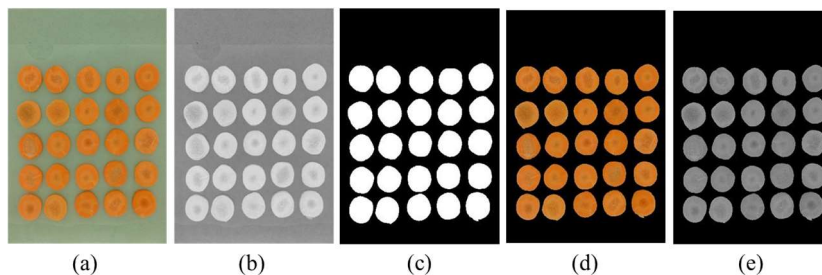


Figure 2. Different stages of an image of fresh carrot slices (5 mm thickness) taken for the experiment, (a) original image; (b) image in the red channel; (c) segmented binary image; (d) masked color image; (e) gray scale image.

Filtering

Filtering is an essential part of image pre-processing. This reduces the noise in the image. Thus, improves the quality and interpretability of images. In this research, a Gaussian filter was used.

Separation of the red band

The red channel of the acquired image is separated from the other two channels namely R (red) and G (green). This was done to improve the result of the segmentation process. The lower redness value of the background and higher redness value of the object makes it convenient to differentiate between these two.

Segmentation

Through image segmentation, the object of interest is separated from the background and other secondary entities^[30]. Then appropriate segmentation method (Otsu method) was used or thresholding operation. Essentially this step separates the object from the background and thus we are left with only an object of interest. This operation results in a binary image with objects assigned with 1 and background

with 0.

Morphological closing

The morphological closing operation is a fundamentally mathematical set operation. It includes firstly erosion and then dilation. These are used for reduction in further noise in the image. Erosion operation removes pixels from the edges of objects in a binary image. While dilation operation fills up the noisy hole within the object of interest. Thus, an image is resulted in removed noises both in boundary and interior. In this particular research disk of the 5-pixel radius was used as a structural element for closing operation.

Area

The area of objects was measured based on the closed foreground of the image. The value returns the total number of pixels, assigned with 1. Now based on the resolution of the image, the returned value was converted into the physical area (mm²). Here 72 dpi means there are 72 pixels in one inch. Also, the number of pixels in horizontal (1920) and vertical directions (2560) is also known. Thus, the area of each pixel was found and finally, the total areas of objects were determined.

Masking with the original image

The masking operation is done to extract the original color object from its background. It is a matrix multiplication operation. The binary image, having only 1 and 0 is multiplied with each of the R, G, B channels of the original image. Thus, the gray level values of objects remain the same whereas values of other background pixels get zero. To get the original image back, three masked channels are catenated together. Thus, we get the original image back in masked form.

Color feature extraction from masked image

Feature extraction, as the name suggests, essentially means quantification of attributes of the image. Image features are mainly classified as external and internal features. External features are the description of the boundary of a region of interest. Internal image features are attributes related to pixels inside the region of interest. The color feature is one of the widely used internal features. It depicts gray level values of each pixel inside the object.

The camera perceives the image in *RGB* color channels. This channel is device-dependent, which means for different acquisition systems like camera scanners etc. *RGB* values will differ. Thus, to get a reproducible result one must convert this value to such values which are not device-dependent. The “Lab” color space is such a space in which values do not depend on the device which captures the image. So, the masked color image is converted into “Lab” using MATLAB codes. The average values of *RGB* and Lab as well are taken as color features in this research.

Conversion of the masked image into gray scale

The masked color image is then converted into a gray scale. This results in an image containing a weighted average of the gray level of *RGB* values in a particular pixel as given in Equation (1).

$$\text{Gray scale value} = 0.2989 \times R + 0.5870 \times G + 0.1140 \times B \quad (1)$$

where *R*, *G*, *B* represents gray level values of each of the red, green, and blue channel in a particular pixel. The gray level scale value represents the weighted average of the aforementioned values. This is done to compute the image texture features in a convenient way. Otherwise, the texture will be computed in each color plane. It will result in unnecessary computation.

Image texture parameters

Like color features, texture features are also important internal features. The idea of texture in computer vision is completely different than the food industry. In the food industry, food texture, such as gumminess, chewiness, brittleness, adhesiveness, elasticity, viscosity, cohesiveness, and, hardness, is generally discussed while in computer vision discuss image texture as graininess, smoothness, coarseness, and fineness, and is generally characterized by the spatial arrangement of the brightness values of the pixels in a region in images^[35]. Texture can reflect the cellular structure of food materials in food images and therefore can be utilized as a food quality indicator up to some extent^[36]. There are different methods to calculate these features like statistical, spectral, and structural. Among all these methods, the statistical texture is the most extensively^[37] applied method in the food industry for classification or quality grading. One of the widely used statistical texture analysis methods is the grey level co-occurrence matrix, in which the texture feature is extracted by some statistical approaches from the co-occurrence matrix^[38]. The relation of pixel gray level intensity with neighboring pixels at a particular distance and direction is computed, called co-occurrence matrix. The statistical relationships of the elements of the co-occurrence matrix are found out. Energy, entropy, homogeneity, etc. are mainly used texture features. Each of these features represents distinct properties of an image.

2.4. Significant feature selection

Extraction of features in large numbers results in so much redundant data. There are many methods, used for data redundancy like filter method, wrapper method, and embedded method. For this current research Boruta algorithm was used^[39]. This algorithm is based on the wrapper method. A random forest classifier is used for the selection of significant features among all attributes. It randomly creates many decision trees based on a different number of attributes and thus creates and thus a random forest from a given data set. It also creates shadow variables from the dataset. Each attribute is given an important value as per the classification accuracy. Now the addition of a new branch in the tree that is a new attribute either results in improved or declined accuracy of the tree. Now the change of the importance of an attribute at different trees is computed. If this importance is widely varied the attribute is marked as important otherwise unimportant.

Recently it has found its place in different fields from remote sensing to medicine. Poona and Ismail^[31] have applied this algorithm for discrimination between stressed and healthy seedlings using hyperspectral data and Boruta was found to be performing best among other used algorithms. Chen et al.^[40] used the Boruta algorithm to find out significant genera of microbes from a pool of microflora causing multiple sclerosis of patients.

2.5. Artificial neural network

Artificial neural network (ANN) is a computing system of interconnected neurons arranged in layers. An input layer, one or more hidden layers, and an output layer are comprised in the feed-forward network. From the outside world, the information is received through the input layer, get processed, and then transmitted to the hidden layers. The predictions get transmitted to the external world by the output layer. "Training" is the iterative process of adjusting the network connection weights in response to a number of examples presented to the network. Training is done to achieve a unique set of connection weights required to compute outputs that are very adjacent to the desired outputs for all the examples used in training^[41-44].

ANN models are generally used for classification, prediction, and clustering. This gives an idea

about the effect of independent drying parameters on the quality of carrots, expressed in terms of image features. Drying time, air temperature, and thickness of carrot slices was kept as input variables. The significant features found from the Boruta algorithm were kept as output variables. The total dataset (378) was divided into training (278) and testing (100) datasets. The ranges of responses were different from one another. This results in slower or early stopping of learning the algorithm. To prevent this situation input and output values were normalized between -1 to +1.

Using MATLAB 2015a Neural Network Toolbox, a multilayer feed forward neural network was formed. Levenberg-Marquardt algorithm was used as a training algorithm. A tan-sigmoid function (Equation (2)) was used as the transfer function in the first layer of the network, and a linear (Equation (3)) function was used in the second layer. While training the network, 70% of the data was used for training, 15% was used for validation to prevent overfitting, and the rest 15% was used for testing the model. Once created, the original test data (100) was fed into the network, and output was simulated. Finally, simulated and experimented responses were plotted to find out the goodness of fit of the network architecture to predict the output.

$$\text{Tansig}(x) = \frac{2}{(1 + e^{-2x})} - 1 \tag{2}$$

$$\text{Purlin}(x) = x \tag{3}$$

Since there is no universally standardized rule for learning rules at input-output layers and the number of hidden layers and neurons at each layer, by trial and error well-performing, suitable architecture was established.

2.6. Data analysis for optimization

All the important responses got from the Boruta algorithm were analyzed. For optimization of processing conditions (hot air temperature and thickness of carrot slice) Design Expert 7.0 (Stat-Ease, USA) software was used, and numerical optimization was employed.

General quadratic second-order polynomial was used for modeling responses with the given set of input variables as shown in (Equation (4)).

$$Y_r = b_{r0} + \sum_{i=1}^2 b_{ri}x_i + \sum_{i=1}^2 b_{rii}x_i^2 + \sum_{i \neq j=1}^2 b_{rij}x_i x_j \tag{4}$$

where: Y_r = Responses selected from Boruta algorithm, and b_0, b_i, b_{ii}, b_{ij} —constants, linear, quadratic, and cross-product regression coefficients, respectively. Numerical optimization was used to optimize selected features using a regression model within the experimental range.

3. Results and discussion

3.1. Kinetics of drying

The variation of moisture ratio of carrot slices (3, 5, 7 mm thicknesses) with different levels of hot air temperatures (60 °C, 70 °C, and 80 °C) are shown in **Figure 3**. It can be found that at a fixed temperature of hot air as the thickness of the slices increased, the drying time increased^[45,46]. It was also observed that at a higher temperature range the drying time was almost similar to each other at different thicknesses of carrot slices. However, a different type result was reported by Doymaz^[47], stating the increase in drying air temperature results in a decrease in the drying time. The observed result in the current study could be attributed to several reasons including the variety of the carrot as it was procured from the local market and could also be thinner thickness selection for the study purpose which led to

faster moisture removal.

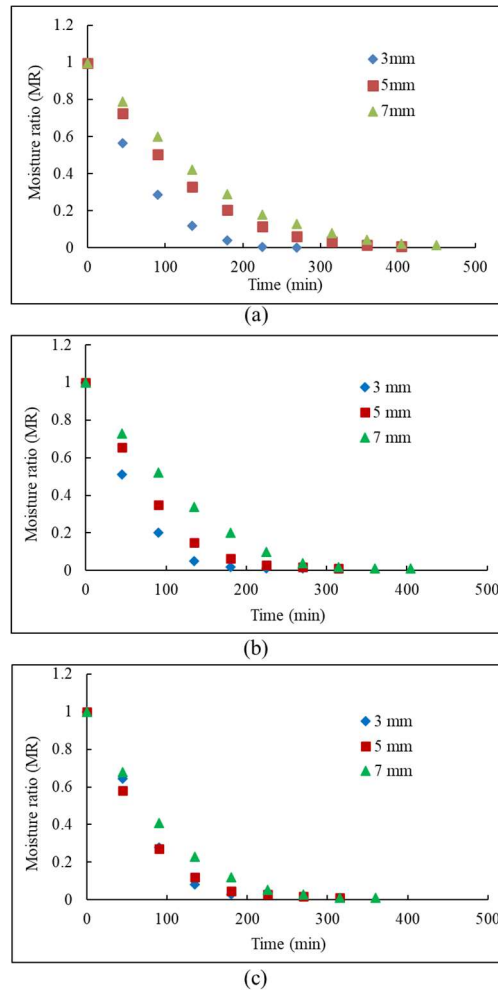


Figure 3. Moisture ratio variation of different thickness carrot slices at hot air temperatures of (a) 60 °C; (b) 70 °C; (c) 80 °C with time.

3.2. Important feature selection

The dataset on which the Boruta algorithm was applied was generated by taking image features at 45 min intervals at different experimental conditions. Features were combined all together and a larger dataset was produced. The codes are written in the R console to analyze the significant features as shown in **Figure 4**. **Figure 5** represents the several significant image attributes in a graphical manner as obtained from the R console. Representation in this fashion improves the interpretability of the results. It can be seen that all the features are selected as important. This is expected because so far these features like area, total color change have been widely used for modeling as response variables^[24,27-29]. But as proposed by Zenoozian et al.^[23], the textural and morphological features should also be taken into account to get a holistic view of the effect of drying on product quality. Here, based on mean importance top three important features were selected as energy, lightness, and redness. These features were further used for ANN modeling and used for optimization as well.

```

R Console
After 10 iterations, +1.5 secs:
confirmed 10 attributes: a, Area, b, B, energy and 5 more;
no more attributes left.

> final.boruta <- TentativeRoughFix(boruta.train)
Warning message:
In TentativeRoughFix(boruta.train) :
  There are no Tentative attributes! Returning original object.
> boruta.df <- attStats(final.boruta)
> print(boruta.df)
  meanImp medianImp minImp maxImp normHits decision
Area  10.503179 10.543887  9.193866 11.426832      1 Confirmed
energy 14.366621 14.717520 12.716122 14.950534      1 Confirmed
L     12.282857 12.432369 11.122494 13.675131      1 Confirmed
a     13.979628 14.239668 11.910750 14.770146      1 Confirmed
b     11.980933 12.006574 10.587678 13.580631      1 Confirmed
R     12.154836 12.312312 11.486548 12.490150      1 Confirmed
G     11.752899 11.749251 11.347796 12.136793      1 Confirmed
B     8.496410  8.317980  8.063084  9.403479      1 Confirmed
entropy 8.787708 8.602785  7.739440 10.036577      1 Confirmed
X.E   8.327685  8.401222  5.928337  9.727014      1 Confirmed
> plot(boruta.train, xlab = "", xaxt = "n")
> lz<-lapply(1:ncol(boruta.train$ImpHistory), function(i)
+ boruta.train$ImpHistory[is.finite(boruta.train$ImpHistory[,i]),i])
> names(lz) <- colnames(boruta.train$ImpHistory)
    
```

Figure 4. Representation of codes written in R console to analyze the significant features.

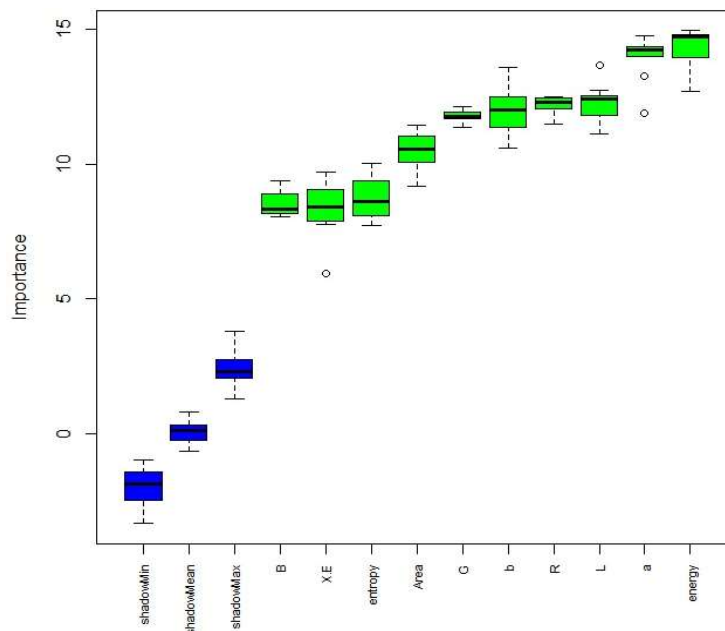


Figure 5. Representation of significant feature attributes in graphical manner as obtained from R console.

3.3. ANN modeling

As mentioned earlier, there is no fixed rule which architecture of the neural network best describes the dataset, the appropriate architecture was figured out by trial and error. Calculation with one hidden layer is less computationally intensive than multiple hidden layers. So, iteration was started with one hidden layer to check it describes the relationship between input and output properly or not. Keeping one hidden layer and transfer function from input fixed number of neurons in the hidden layer was changed. Firstly, the log sigmoid transfer function was used to relate the hidden layer to output. The performance of different neural network architectures with one hidden layer is given in **Table 1**, as observed from the table the simulated output with mean square error (MSE) is around 0.59. As the data is normalized between -1 to +1, MSE in this order cannot be tolerated. Then pure linear transfer function was used to

associate the hidden layer to output. The number of neurons was varied among 3, 5, 7, and 10. The least MSE was found in architecture consisting of 7 neurons. The MSE of the testing set was found to be 0.026. This result is good to be considered. Thus, further hidden layers were not increased. **Table 2** shows the characteristics of selected ANN architecture.

Table 1. Performance of different neural network architectures with one hidden layer.

Simulation	Transfer function from input to hidden layer	Transfer function into the output from the hidden layer	Number of neurons	Mean square error (MSE)	
				Training set	Testing set
1	Tan sigmoid	Log-sigmoid	3	0.256	0.593
2	Tan sigmoid	Log-sigmoid	5	0.260	0.597
3	Tan sigmoid	Pure linear	3	0.014	0.045
4	Tan sigmoid	Pure linear	5	0.012	0.048
5	Tan sigmoid	Pure linear	7	0.015	0.026
6	Tan sigmoid	Pure linear	10	0.016	0.028

Table 2. Structure characteristics of ANN architecture.

Structural characteristics	ANN architecture
Neural network architecture	3-7-3
Total number of hidden layers	1
Number of nodes in input layer	3
Number of nodes in output layer	7
Number of nodes in hidden layer	3
Transfer function from input to hidden layer	Tan sigmoid
Transfer function to output from hidden layer	Pure linear

Simulated results of selected ANN architecture

The simulated values of normalized predicted and experimented outputs are shown in **Figure 6** using neural network architecture with seven neurons in one hidden layer. Outputs of the networks, energy, lightness, redness of dried carrot slices were fairly congruent with experimental values ($R^2 = 0.94, 0.94, 0.91$) respectively. This is correlating with the capacity of ANN as a modeling tool for nonlinear data.

The weight matrix of the hidden layer (IW) and the output layer (LW) and the bias of hidden layer (b^1) and output layer (b^2) showed the following values in Equations (5–8):

$$IW = \begin{bmatrix} 0.15488 & -0.56547 & -3.9113 \\ -2.0462 & -2.1848 & -1.5131 \\ -0.03037 & -0.85566 & 0.50453 \\ -0.12173 & 0.32794 & -3.0308 \\ 3.232 & 1.6069 & -2.6334 \\ -1.2637 & -2.0799 & 0.73162 \\ 3.3525 & -1.842 & -2.0704 \end{bmatrix} \quad (5)$$

$$LW = \begin{bmatrix} 0.45048 & 0.13598 & -0.52363 & 0.34219 & -0.17151 & -0.27104 & 0.12353 \\ -0.39676 & -0.11841 & 0.42143 & -0.39751 & 0.15787 & 0.31384 & -0.09671 \\ 0.39507 & 0.050292 & -0.32338 & 0.30661 & -0.15527 & -0.26123 & 0.12888 \end{bmatrix} \quad (6)$$

$$(b^1) = \begin{bmatrix} -3.4832 \\ 0.32809 \\ 0.8263 \\ -1.2111 \\ 1.2943 \\ -2.4073 \\ 3.9102 \end{bmatrix} \quad (7)$$

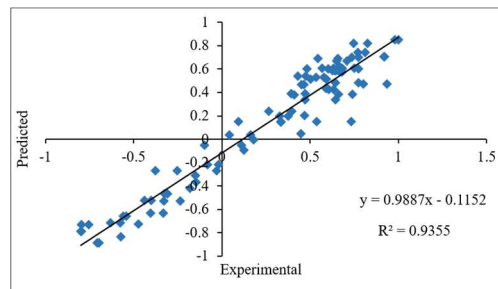
$$(b^2) = \begin{bmatrix} 0.074467 \\ -0.10062 \\ -0.16371 \end{bmatrix} \quad (8)$$

Depending on the developed architecture, the model of neural network which was used for describing the kinetics of drying of carrot slices can be written as the following equation (Equation (9)).

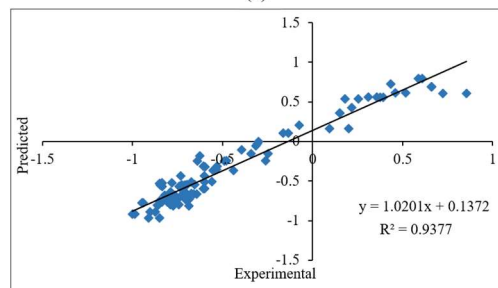
$$\text{Output} = \text{Purelin} [LW \times \text{Tansig} (IW \times \text{inputs} + b^1) + b^2] \quad (9)$$

Equation (9) can be simplified as Equation (10).

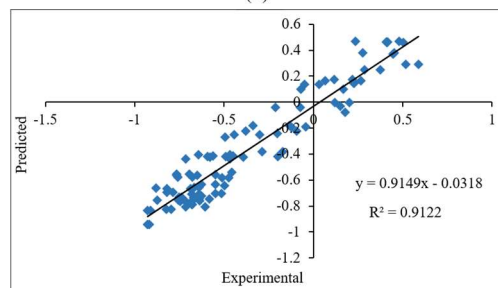
$$\text{Output} = LW \times \left\{ \frac{2}{1 + e^{(-2 \times (IW \times \text{inputs} + b^1))}} - 1 \right\} + b^2 \quad (4)$$



(a)



(b)



(c)

Figure 6. Predicted vs. experimented plot of (a) normalized energy; (b) lightness; (c) normalized redness values of dried carrot slices.

3.4. Response of the experiments

The effect of convective hot air temperature and thickness of carrot slices on responses such as energy, lightness, and redness are shown in **Table 3**. It can be observed that responses did not vary much

among different operating conditions. The variations in response variables, depending upon the inputs, are discussed in detail.

Table 3. The effect of convective hot air temperature and thickness of carrot slices on responses such as energy, lightness, and redness.

Temperature (°C)	Thickness (mm)	Energy	Lightness	Redness
60	3	0.84	13.79	29.21
60	5	0.82	14.13	29.69
60	7	0.81	14.55	30.14
70	3	0.85	12.91	28.59
70	5	0.83	13.56	29.01
70	7	0.82	13.75	29.21
80	3	0.89	11.67	27.85
80	5	0.86	11.86	28.39
80	7	0.83	12.29	28.65

3.5. Regression modeling of responses

Statistical analysis was performed to find out the significance of independent parameters i.e., convective air temperature and carrot slice thickness on responses, such as Energy, lightness, and redness. Multiple regression was performed, and coefficients of regression were found to assess the behavior of responses as the function of inputs. ANOVA (Table 4) was performed on each of the responses on the experimented dataset and significant terms were determined based on *F*-value. Model adequacies were checked by *R*², adjusted-*R*², and predicted-*R*². The coefficient of variation was used to figure out the dispersion of data. CV was found to be below 5. It indicates that drying temperature and slice thickness significantly affect the energy, lightness, and redness in the convective hot air-drying process. Despite the fact that the quadratic model was fitted to all three responses, energy (adjusted-*R*² = 0.89) and lightness (adjusted-*R*² = 0.95) was modeled well in the linear model. Whereas redness was well described as a quadratic model (adjusted-*R*² = 0.98). The coefficients of multiple regression of responses (energy, lightness, and redness) are listed in Table 5.

Table 4. Results of ANOVA analysis on response variables such as energy, lightness, redness.

Source	Energy			Lightness			Redness		
	Sum of squares	df	<i>p</i> -value prob. > <i>F</i>	Sum of squares	df	<i>p</i> -value prob. > <i>F</i>	Sum of squares	df	<i>p</i> -value prob. > <i>F</i>
Model	0.0035	2	0.0006	8.2162	2	<0.0001	3.8190	5	0.0018
<i>A</i> —temperature	0.0012	1	0.0029	7.3922	1	<0.0001	2.8805	1	0.0004
<i>B</i> —thickness	0.0022	1	0.0006	0.8239	1	0.0073	0.9115	1	0.0019
<i>AB</i>	-	-	-	-	-	-	0.0043	1	0.5245
<i>A</i> ²	-	-	-	-	-	-	0.0059	1	0.4654
<i>B</i> ²	-	-	-	-	-	-	0.0166	1	0.2568
Residuals	0.0003	6	-	0.3120	6	-	0.0255	3	-
Cor. total	0.0038	8	-	8.5282	8	-	3.8445	8	-
Std. Dev.	0.0072	-	-	0.2280	-	-	0.0922	-	-
Mean	0.8397	-	-	13.1671	-	-	28.9723	-	-

Table 4. (Continued).

Source	Energy			Lightness			Redness		
	Sum of squares	df	p-value prob. > F	Sum of squares	df	p-value prob. > F	Sum of squares	df	p-value prob. > F
C.V. %	0.8661	-	-	1.7318	-	-	0.3184	-	-
Press	0.0008	-	-	0.5579	-	-	0.3096	-	-
R ²	0.9172	-	-	0.9634	-	-	0.9933	-	-
Adj-R ²	0.8897	-	-	0.9512	-	-	0.9822	-	-
Pred-R ²	0.7836	-	-	0.9345	-	-	0.9194	-	-
Adeq precision	16.1236	-	-	22.4897	-	-	28.7463	-	-

Note: df—degree of freedom, Prob—Probability, F—F-value, Cor.—correlation, Std. Dev.—Standard deviation, C.V.—Coefficient of variation, Adj—Adjusted, Pred—Predicted, Adeq—Adequacy.

Table 5. Coefficients of multiple regression of energy, lightness, and redness.

Factors	Energy	Lightness	Redness
	Coefficient estimate	Coefficient estimate	Coefficient estimate
Intercept	0.83973	13.16798	28.99679
A—temperature	0.01431	-1.10998	-0.69289
B—thickness	-0.01954	0.37058	0.38977
AB	-	-	-0.03313
A ²	-	-	0.05442
B ²	-	-	-0.09113

3.5.1. Effect of temperature on energy response

Figure 7a shows the effect of temperature and thickness on energy. It can be found that energy is increases as the temperature increases. It also increases with reduced thickness. The effect of thickness on energy was more pronounced than that of temperature. This increase in energy could be related to smaller pores, leading to a uniform and regular structure.

3.5.2. Effect of temperature on lightness response

The effect of temperature (45–65 °C) in lightness and redness of carrot slices (7 ± 1 mm) thickness was previously investigated by Demiray and Tulek^[48]. They have found that at lightness value after drying at 55–65 °C varied between 49.32 and 51. This difference of lightness among different temperatures was decreased at a higher temperature range. In the current study, the experiments were carried even higher range. This results in almost close values of lightness. Although in the literature studied, the effect of thickness on lightness was not investigated, it was found that lightness increased, with increased thickness. The effect of temperature and thickness on lightness is given in Figure 7b, demonstrating with greater thickness, the severity of the heating was reduced. The values were close to each other. In this research, lightness values were much lower than the lightness values found by Demiray and Tulek^[48], which could be a result due to the variety of carrots.

3.5.3. Effect of temperature on redness response

The decreased redness of carrot slices can be associated with the degradation of β-carotene with intensified heating effect. The redness values of carrot slices after drying at 55–65 °C were close to each other, around 31^[48]. In this research, it was found to be varying between 28 and 30. With higher temperatures, redness was found to be reduced (Figure 7c). In the same time with higher thickness, it was found to be decreased. With greater thickness, the area exposed to heating medium per unit mass was lesser, thus the retention of β-carotene was greater. This resulted in greater redness.

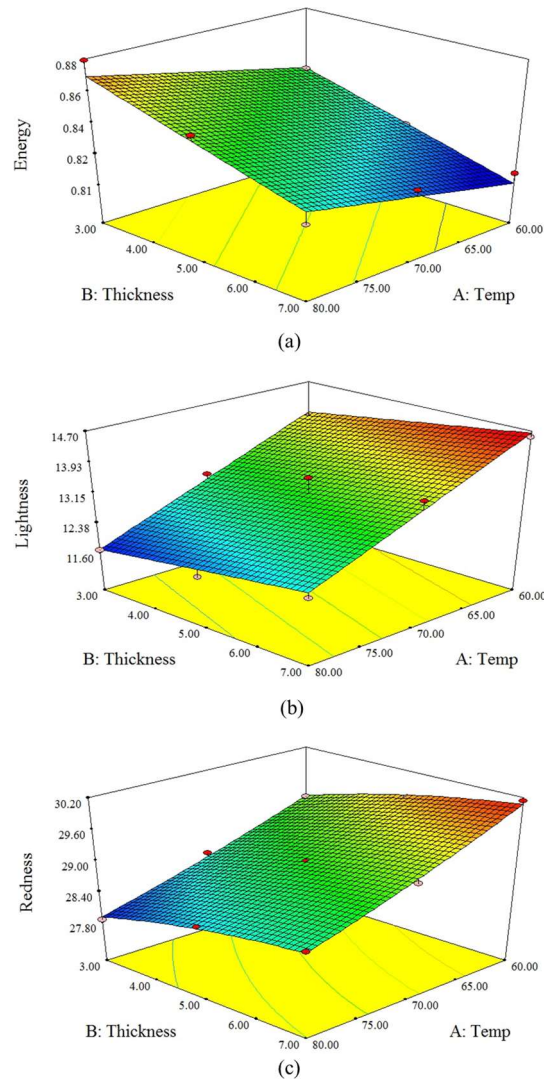


Figure 7. Surface plot of temperature and thickness vs. (a) energy; (b) lightness; and (c) redness of dried carrot slices.

3.6. Optimization of operating conditions of hot air drying

Predictive models of response, energy, lightness, redness was further used to optimize the drying conditions, the thickness of carrot slices, and temperature of convective hot air. These regression models of responses were only valid within experimental limits. Optimization of convective hot air drying for carrots was conducted to minimize energy and maximize lightness and redness. The energy was minimized to lessen the uniformity of the surface of slices. The dried carrot surface has more uniformity thus the energy of the acquired image is higher. The constraints for numerical optimization are given in **Table 6**. The thickness of slices and temperature of convective hot air was kept within limits. The optimal values of hot air temperature and carrot slice thickness were 60 °C and 7 mm with a desirability of 0.87. Besides, the response variables such as energy, lightness, and redness were found to be 0.83, 14.64, and 30.07 respectively.

Table 6. Constrains for numerical optimization for thickness of slices, and temperature of convective hot air, and responses.

Name	Goal	Lower limit	Upper limit	Lower weight	Upper weight	Importance
Temperature	is in range	60	80	1	1	3
Thickness	is in range	3	7	1	1	3
Energy	minimize	0.81	0.88	1	1	3
Lightness	maximize	11.66	14.55	1	1	3
Redness	maximize	27.85	30.14	1	1	3

4. Conclusion

Images of dried carrot slices were taken during the various condition of drying. These were then analyzed and different image features were got. Statistically, significant features among all the analyzed responses were found out using the Boruta algorithm. The artificial neural network was used to assess the effects of drying conditions (drying time, hot air temperature, thickness of carrot slices) on the selected image features (lightness, redness, energy). Predicted outputs of the networks, lightness, energy, redness of dried carrot slices was in good agreement with experimental values ($R^2 = 0.94, 0.94, 0.91$) respectively. Further drying condition (air temperature and thickness of slice) was optimized based on features. Lightness and redness were set to be maximized whereas energy was to be minimized. Optimized drying condition was found to be 60 °C and carrot slice thickness of 7 mm. From the current research findings, it can be observed that the energy, a measure of uniformity of surface increased with an increase in severity of drying conditions. The lightness and redness decreased with an increase in the severity of the drying condition. The lowest temperature of hot air and highest thickness of carrot slice produce the best quality of the product within the experimental range of operation. Therefore, the current research can help the food industries in understanding the distribution of quality attributes of agricultural commodities in a non-destructive way and maintaining them as needed.

Author contributions

Conceptualization, GB and KD; methodology, GB and KD; software, GB; validation, GB and KD; formal analysis, GB and KD; investigation, GB and KD; resources, GB and KD; data curation, GB and KD; writing—original draft preparation, GB and KD; writing—review and editing, KD, PPT, and SS; visualization, GB and KD; supervision, PPT; project administration, GB and KD; funding acquisition, PPT. All authors have read and agreed to the published version of the manuscript.

Acknowledgments

The authors are grateful to the Indian Institute of Technology Kharagpur for infrastructure and facilities to conduct the research.

Conflict of interest

The authors declare no conflict of interest.

References

1. Food and Agriculture Organization of the United Nations Carrots and Turnips, 2020. Available online: <http://www.fao.org/faostat/en/#data/QC/visualize>. (Accessed on 10 October 2022).
2. Ahmad T, Cawood M, Iqbal Q, et al. Phytochemicals in *Daucus carota* and Their Health Benefits. *Foods*. 2019; 8(9): 424. doi: 10.3390/foods8090424
3. Dhalsamant K, Tripathy PP, Shrivastava SL. Effect of pretreatment on rehydration, colour and

- nanoindentation properties of potato cylinders dried using a mixed - mode solar dryer. *Journal of the Science of Food and Agriculture*. 2017; 97(10): 3312–3322. doi: 10.1002/jsfa.8181
4. Wang H, Fang XM, Sutar PP, et al. Effects of vacuum-steam pulsed blanching on drying kinetics, colour, phytochemical contents, antioxidant capacity of carrot and the mechanism of carrot quality changes revealed by texture, microstructure and ultrastructure. *Food Chemistry*. 2021; 338: 127799. doi: 10.1016/j.foodchem.2020.127799
 5. Sharma S, Dhalsamant K, Tripathy PP. Application of computer vision technique for physical quality monitoring of turmeric slices during direct solar drying. *Journal of Food Measurement and Characterization*. 2018; 13(1): 545-558. doi: 10.1007/s11694-018-9968-0
 6. Sharma S, Dhalsamant K, Tripathy PP, et al. Quality analysis and drying characteristics of turmeric (*Curcuma longa* L.) dried by hot air and direct solar dryers. *LWT*. 2021; 138: 110687. doi: 10.1016/j.lwt.2020.110687
 7. Mudahar GS, Toledo RT, Floros JD, et al. Optimization of Carrot Dehydration Process using Response Surface Methodology. *Journal of Food Science*. 1989; 54(3): 714-719. doi: 10.1111/j.1365-2621.1989.tb04688.x
 8. Dey D, Dhalsamant K, Tripathy PP. Effect of different pre-treatments on rehydration kinetics of solar and hot-air dried Fuji apple slices. *Trends in Horticulture*. 2023; 6(2): 3185. doi: 10.24294/th.v6i2.3185
 9. Kakani V, Nguyen VH, Kumar BP, et al. A critical review on computer vision and artificial intelligence in food industry. *Journal of Agriculture and Food Research*. 2020; 2: 100033. doi: 10.1016/j.jafr.2020.100033
 10. Jahanbakhshi A, Kheiralipour K. Evaluation of image processing technique and discriminant analysis methods in postharvest processing of carrot fruit. *Food Science & Nutrition*. 2020; 8(7): 3346-3352. doi: 10.1002/fsn3.1614
 11. Tian H, Wang T, Liu Y, et al. Computer vision technology in agricultural automation —A review. *Information Processing in Agriculture*. 2020; 7(1): 1-19. doi: 10.1016/j.inpa.2019.09.006
 12. Zhu H, Yang L, Sun Y, et al. Identifying carrot appearance quality by an improved dense CapNet. *Journal of Food Process Engineering*. 2020; 44(1). doi: 10.1111/jfpe.13586
 13. Mohebbi M, Akbarzadeh-T MR, Shahidi F, et al. Computer vision systems (CVS) for moisture content estimation in dehydrated shrimp. *Computers and Electronics in Agriculture*. 2009; 69(2): 128-134. doi: 10.1016/j.compag.2009.07.005
 14. Aghbashlo M, Hosseinpour S, Mujumdar AS. Application of Artificial Neural Networks (ANNs) in Drying Technology: A Comprehensive Review. *Drying Technology*. 2015; 33(12): 1397-1462. doi: 10.1080/07373937.2015.1036288
 15. El-Mesery H, Mao H, Abomohra A. Applications of Non-destructive Technologies for Agricultural and Food Products Quality Inspection. *Sensors*. 2019; 19(4): 846. doi: 10.3390/s19040846
 16. Ebrahimi E, Mollazade K, Babaei S. Toward an automatic wheat purity measuring device: A machine vision-based neural networks-assisted imperialist competitive algorithm approach. *Measurement*. 2014; 55: 196-205. doi: 10.1016/j.measurement.2014.05.003
 17. Sampson DJ, Chang YK, Rupasinghe HPV, et al. A dual-view computer-vision system for volume and image texture analysis in multiple apple slices drying. *Journal of Food Engineering*. 2014; 127: 49-57. doi: 10.1016/j.jfoodeng.2013.11.016
 18. Majumdar S, Jayas DS. Classification of cereal grains using machine vision: IV. Combined morphology, color, and texture models. *Transactions of the ASAE*. 2000; 43(6): 1689-1694. doi: 10.13031/2013.3069
 19. Zhang Y, Wang S, Ji G, et al. Fruit classification using computer vision and feedforward neural network. *Journal of Food Engineering*. 2014; 143: 167-177. doi: 10.1016/j.jfoodeng.2014.07.001
 20. Fathi M, Mohebbi M, Razavi SMA. Application of Image Analysis and Artificial Neural Network to Predict Mass Transfer Kinetics and Color Changes of Osmotically Dehydrated Kiwifruit. *Food and Bioprocess Technology*. 2009; 4(8): 1357-1366. doi: 10.1007/s11947-009-0222-y
 21. Hosseinpour S, Rafiee S, Mohtasebi SS. Application of Image Processing to Analyze Shrinkage and Shape Changes of Shrimp Batch during Drying. *Drying Technology*. 2011; 29(12): 1416-1438. doi: 10.1080/07373937.2011.587620
 22. Hosseinpour S, Rafiee S, Mohtasebi SS, et al. Application of computer vision technique for on-line monitoring of shrimp color changes during drying. *Journal of Food Engineering*. 2013; 115(1): 99-114. doi: 10.1016/j.jfoodeng.2012.10.003
 23. Zenoozian MS, Feng H, Razavi SMA, et al. Image analysis and dynamic modeling of thin-layer drying of osmotically dehydrated pumpkin. *Journal of Food Processing and Preservation*. 2008; 32(1): 88-102. doi: 10.1111/j.1745-4549.2007.00167.x
 24. Sturm B, Hofacker WC, Hensel O. Optimizing the Drying Parameters for Hot-Air-Dried Apples. *Drying Technology*. 2012; 30(14): 1570-1582. doi: 10.1080/07373937.2012.698439
 25. Jahns G, Nielsen HM, Paul W. Measuring image analysis attributes and modelling fuzzy consumer aspects

- for tomato quality grading. *Comput. Electron. Agric.* 2001; 31(1): 17-29. doi: 10.1016/S0168-1699(00)00171-X
26. Blaschke T. Object based image analysis for remote sensing. *ISPRS Journal of Photogrammetry and Remote Sensing.* 2010; 65(1): 2-16. doi: 10.1016/j.isprsjprs.2009.06.004
 27. Behroozi Khazaei N, Tavakoli T, Ghassemian H, et al. Applied machine vision and artificial neural network for modeling and controlling of the grape drying process. *Computers and Electronics in Agriculture.* 2013; 98: 205-213. doi: 10.1016/j.compag.2013.08.010
 28. Dhalsamant, K., Tripathy, P. P., & Shrivastava, S. L. (2017). Moisture transfer modeling during solar drying of potato cylinders considering shrinkage. *International Journal of Green Energy*, 14(2), 184-195. doi: 10.1080/15435075.2016.1256290
 29. Hosseinpour S, Rafiee S, Aghbashlo M, et al. Computer Vision System (CVS) for In-Line Monitoring of Visual Texture Kinetics During Shrimp (*Penaeus Spp.*) Drying. *Drying Technology.* 2014; 33(2): 238-254. doi: 10.1080/07373937.2014.947513
 30. Fernandez L, Castellero C, Aguilera JM. An application of image analysis to dehydration of apple discs. *Journal of Food Engineering.* 2005; 67(1-2): 185-193. doi: 10.1016/j.jfoodeng.2004.05.070
 31. Poona NK, Ismail R. Using Boruta-Selected Spectroscopic Wavebands for the Asymptomatic Detection of *Fusarium Circinatum* Stress. *IEEE Journal of Selected Topics in Applied Earth Observations and Remote Sensing.* 2014; 7(9): 3764-3772. doi: 10.1109/jstars.2014.2329763
 32. Lim DK, Long NP, Mo C, et al. Combination of mass spectrometry-based targeted lipidomics and supervised machine learning algorithms in detecting adulterated admixtures of white rice. *Food Research International.* 2017; 100: 814-821. doi: 10.1016/j.foodres.2017.08.006
 33. Min W, Zhou P, Xu L, et al. From Plate to Production: Artificial Intelligence in Modern Consumer-Driven Food Systems. arXiv preprint arXiv:2311.02400
 34. Banda T, Farid AA, Li C, et al. Application of machine vision for tool condition monitoring and tool performance optimization—a review. *The International Journal of Advanced Manufacturing Technology.* 2022; 121(11-12): 7057-7086. doi: 10.1007/s00170-022-09696-x
 35. Zheng C, Sun DW, Zheng L. Recent applications of image texture for evaluation of food qualities—A review. *Trends in Food Science & Technology.* 2006; 17(3): 113-128. doi: 10.1016/j.tifs.2005.11.006
 36. Gao X, Tan J. Analysis of expanded - food texture by image processing part II: Mechanical properties. *Journal of Food Process Engineering.* 1996; 19(4): 445-456. doi: 10.1111/j.1745-4530.1996.tb00404.x
 37. Brosnan T, Sun DW. Improving quality inspection of food products by computer vision—A review. *J. Food Eng.* 2004; 61: 3-16. doi: 10.1016/S0260-8774(03)00183-3
 38. Haralick RM, Shanmugam K, Dinstein I. Textural Features for Image Classification. *IEEE Transactions on Systems, Man, and Cybernetics.* 1973; SMC-3(6): 610-621. doi: 10.1109/tsmc.1973.4309314
 39. Kursu MB, Rudnicki WR. Feature Selection with the Boruta Package. *Journal of Statistical Software.* 2010; 36(11). doi: 10.18637/jss.v036.i11
 40. Chen J, Chia N, Kalari KR, et al. Multiple sclerosis patients have a distinct gut microbiota compared to healthy controls. *Scientific Reports.* 2016; 6(1). doi: 10.1038/srep28484
 41. Chen CR, Ramaswamy HS, Alli I. Prediction of quality changes during osmo-convective drying of blueberries using neural network models for process optimization. *Drying Technology.* 2001; 19(3-4): 507-523. doi: 10.1081/drt-100103931
 42. Cheng F, Chen FN, Ying YB. Image Recognition of Unsound Wheat Using Artificial Neural Network. 2010 Second WRI Global Congress on Intelligent Systems. Published online December 2010. doi: 10.1109/gcis.2010.220
 43. Uhlig S, Colson B, Hettwer K, et al. Valid machine learning algorithms for multiparameter methods. *Accreditation and Quality Assurance.* 2019; 24(4): 271-279. doi: 10.1007/s00769-019-01384-w
 44. Dhalsamant K. Development, validation, and comparison of FE modeling and ANN model for mixed - mode solar drying of potato cylinders. *Journal of Food Science.* 2021; 86(8): 3384-3402. doi: 10.1111/1750-3841.15847
 45. Dhalsamant K, Tripathy PP, Shrivastava SL. Effect of sodium metabisulfite pretreatment on micrographs, surface roughness and X-ray diffraction analyses of solar dried potato cylinders. *Innovative Food Science & Emerging Technologies.* 2018; 47: 399-411. doi: 10.1016/j.ifset.2018.03.014
 46. Dhalsamant K, Tripathy PP, Shrivastava SL. Heat transfer analysis during mixed-mode solar drying of potato cylinders incorporating shrinkage: Numerical simulation and experimental validation. *Food and Bioprocess Processing.* 2018; 109: 107-121. doi: 10.1016/j.fbp.2018.03.005
 47. Doymaz I. Drying kinetics, rehydration and colour characteristics of convective hot-air drying of carrot slices. *Heat and Mass Transfer.* 2016; 53(1): 25-35. doi: 10.1007/s00231-016-1791-8
 48. Demiray E, Tulek Y. Color Degradation Kinetics of Carrot (*Daucus carota* L.) Slices during Hot Air Drying. *Journal of Food Processing and Preservation.* 2014; 39(6): 800-805. doi: 10.1111/jfpp.12290